Check for updates

Molecular composition of fresh and aged aerosols from residential wood combustion and gasoline car with modern emission mitigation technology†

Eric Schneider,[ab] Hendryk Czech, [ID] *[ac] Anni Hartikainen, [ID] [d] Helly J. Hansen,[a] Nadine Gawlitta, [ID] [c] Mika Ihalainen,[d] Pasi Yli-Pirilä,[d] Markus Somero,[d] Miika Kortelainen, [ID] [d] Juho Louhisalmi,[d] Jürgen Orasche, [ID] ‡[c] Zheng Fang,[e] Yinon Rudich, [ID] [e] Olli Sippula,[df] Christopher P. Rüger[ab] and Ralf Zimmermann[abc]

Emissions from road traffic and residential heating contribute to urban air pollution. Advances in emission reduction technologies may alter the composition of emissions and affect their fate during atmospheric processing. Here, emissions of a gasoline car and a wood stove, both equipped with modern emission mitigation technology, were photochemically aged in an oxidation flow reactor to the equivalent of one to five days of photochemical aging. Fresh and aged exhausts were analyzed by ultrahigh resolution mass spectrometry. The gasoline car equipped with a three-way catalyst and a gasoline particle filter emitted minor primary fine particulate matter (PM2.5), but aging led to formation of particulate low-volatile, oxygenated and highly nitrogen-containing compounds, formed from volatile organic compounds (VOCs) and gases incl. NO_x, SO_2, and NH_3. Reduction of the particle concentration was also observed for the application of an electrostatic precipitator with residential wood combustion but with no significant effect on the chemical composition of PM2.5. Comparing the effect of short and medium photochemical exposures on PM2.5 of both emission sources indicates a similar trend for formation of new organic compounds with increased carbon oxidation state and nitrogen content. The overall bulk compositions of the studied emission exhausts became more similar by aging, with many newly formed elemental compositions being shared. However, the presence of particulate matter in wood combustion results in differences in the molecular properties of secondary particles, as some compounds were preserved during aging.

Environmental significance

Epidemiological insights into the relation between levels of fine particulate matter (PM2.5) and public health lead to stricter emissions regulations for residential heating and road traffic, which are significant PM2.5 sources worldwide. For compliance, manufacturers improve combustion technology and develop new emission mitigation strategies, which alter emissions composition compared to older emission sources, with possible impacts on their behavior during atmospheric aging. Laboratory-aging of urban combustion emissions of state-of-the-art devices and subsequent PM2.5 analysis with complementary ultrahigh resolution mass spectrometry techniques shed light on the consequences of technological developments for the atmospheric fate and the composition of the emissions on a molecular level and the consequent changes in particle properties regarding oxidation, aromaticity, and volatility.

[a]Joint Mass Spectrometry Centre, Department of Analytical and Technical Chemistry, University of Rostock, Rostock, Germany. E-mail: hendryk.czech@uni-rostock.de

[b]Department Life, Light & Matter (LL&M), University of Rostock, Rostock, Germany

[c]Joint Mass Spectrometry Centre, Cooperation Group "Comprehensive Molecular Analytics" (CMA), Helmholtz Centre Munich, Munich, Germany

[d]Department of Environmental and Biological Sciences, University of Eastern Finland, Kuopio, Finland

[e]Department of Earth and Planetary Sciences, Weizmann Institute of Science, Rehovot, Israel

[f]Department of Chemistry, University of Eastern Finland, Joensuu, Finland

† Electronic supplementary information (ESI) available. See DOI: https://doi.org/10.1039/d4em00106k

‡ Now at: Chair of Environmental Medicine, University of Augsburg, Augsburg, Germany.

1. Introduction

Combustion emissions contribute significantly to air pollution by releasing airborne fine and coarse particulate matter (PM2.5 and PM10) as well as nitrogen oxides (NO_x) to the atmosphere. Consequently, they pose a threat to public health, linked to respiratory or cardiovascular diseases and an overall increase in premature mortality.[1–5] In the last decades, countermeasures have been applied to reduce health-relevant emissions from road traffic and residential heating with wood, as those have been frequently identified as main sources of ambient PM2.5 or PM10.[6–9] In addition to the three-way and oxidation catalysts for

gasoline and diesel vehicles, particle filters have become more established to comply with stricter exhaust emission standards to reduce tailpipe emissions.[10,11] Furthermore, the addition of oxygen-containing bioethanol or fatty acid methyl esters to gasoline and diesel, respectively, suppresses soot particle formation and consequently diminishes PM2.5 emissions.[12,13] For continuously and batchwise fired residential wood combustion appliances, the development of a secondary air supply by air staging may substantially reduce PM2.5, organic carbon (OC), CO and, for continuously operated appliances, NO_x emissions because of improved oxidation of carbonaceous aerosols and improved availability of NO_x that acts as an oxidant in fuel-rich combustion zones.[14–17]

Atmospheric processing (i.e., 'aging') of aerosols in the presence of NO_x produces photochemical air pollution by increasing urban PM and ground-level ozone concentrations, which is a long-term phenomenon in megacities such as Los Angeles, Mexico City or Beijing, Shanghai, Xi'an, and Guangzhou.[18–20] Gases in primary emissions are oxidized by the atmospheric oxidants, mainly hydroxyl radicals, ozone, and nitrate radicals, and low volatility reaction products may partition to the particle phase.[21,22] Moreover, peroxyalkyl radical ($RO_2^{\cdot}$) intermediates from the atmospheric degradation of organic vapors may oxidize NO, forming NO_2.[23] During daytime, photolysis of NO_2 and produces triplet oxygen $O(^3P)$, which reacts with molecular oxygen to form ozone.[24] Therefore, secondary air pollutants must be considered for an integrated assessment of air pollution control strategies. However, both ground-level ozone and secondary PM formation depend on the aerosol composition, which vary depending on atmospheric conditions such as relative humidity, the ratio of volatile organic compounds (VOC) to NO_x, and light availability (e.g., day- or night time).

Residential wood combustion and traffic emissions, namely gasoline-fueled vehicles (e.g., cars and scooters), contain substantial potential for secondary PM formation, including both secondary organic and inorganic aerosol particles (SOA, SIA).[25–29] Aged emissions from individual primary sources including cars,[30] residential wood combustion,[31] and single combustion-related products like naphthalene[32] or hydrocarbon/NO_x mixtures[33] show distinct effects in in vitro and in vivo models regarding several biological endpoints, such as induction of oxidative stress, genotoxicity, cytotoxicity as well as inflammatory effects. Moreover, also epidemiological findings emphasize the negative effect of SOA on public health by linking SOA to the rate of cardiorespiratory mortality in the United States.[34]

Motivated by stricter legislation, improved combustion technologies or emission mitigation strategies reduce emissions of the regulated species. However, they may also induce changes in emission composition and alter the atmospheric transformation of the emissions. This study characterizes the chemical changes in the composition of particulate emissions of a gasoline car and a residential wood stove, both equipped with commercial state-of-the-art emission mitigation technologies, after photochemical aging in a high-volume oxidation flow reactor. To understand the changes that occur in organic emissions during atmospheric aging, ultrahigh resolution Fourier-transform ion cyclotron resonance mass spectrometry (FT-ICR MS) in combination with atmospheric pressure photoionization (APPI) and electrospray ionization (ESI) provides complementary insights into non-/low-polar and polar organic compounds, respectively.

2. Materials and methods

2.1. Emission sources and laboratory-aging

Wood stove emissions were generated by the combustion of five consecutive batches 2 kg of beech logwood in a modern non-heat-retaining chimney stove (Aduro 9.3, Denmark). Each of the individual batches lasted for 35 min while the combustion experiment was completed by a residual char-burning phase of 30 min as described previously elsewhere.[35] In some of the wood stove experiments, the primary particle emissions were filtered by a tube-type electrostatic precipitator (ESP; OekoTube, Oeko-Solve AG, Switzerland), located on the chimney of the oven, with PM1 reduction efficiencies of 80–97%.[36]

Gasoline car emissions were generated by a turbocharged light-duty gasoline direct injection (GDI) passenger vehicle (Skoda Scala 1.0 TSI, model year 2021) on a chassis dynamometer (Rototest VPA-RX3 2WD). The car was equipped with a three-way catalyst and a gasoline particle filter (GPF), and was compliant with the EURO-6 exhaust emission standard. It was operated with commercial gasoline–ethanol blend fuel 95 E10 (gasoline with max. 10% ethanol content) under the following cycle: cold start and idling for 5 min (no gear), 50 km h^{-1} for 15 min (4th gear), 100 km h^{-1} for 15 min (5th gear), 80 km h^{-1} for 15 min (5th gear) and idling for 5 min (no gear), which was repeated four times. More information about the gases, VOC and organic aerosol emissions can be found elsewhere.[37]

Fresh aerosol emissions were diluted by either a factor of 17 (gasoline car) or 60 (wood stove) by a porous tube ejector dilutor (Venacontra, Finland) before sampling or laboratory aging. PM2.5 of fresh and aged emissions were collected on pre-conditioned quartz fiber filters (47 mm, Munktell) over the total experimental duration of 240 min with a flow of 10 or 5 L min^{-1}, respectively.

Photochemical processing was conducted with the Photochemical Emission Aging flow tube Reactor (PEAR),[38] which is a high-flow oxidation flow reactor with a laminar flow, designed for the aging of transient combustion exhausts. The PEAR was operated with a total flow rate of 130 L min^{-1}. Relative humidity and temperature were 57 ± 6% and 25 ± 2 °C downstream the PEAR. Different photochemical ages were achieved by varying the photon flux at 254 nm through different UV lamp voltages. Initial ozone input to the PEAR was 9 ppm, and hydroxyl radicals (OH) were created by the rapid photolysis of ozone to excited singlet oxygen, which subsequently reacted with water to form OH. OH exposure (OH_{exp}) was traced from the consumption of externally input d9-butanol, monitored by a proton transfer reactor mass spectrometer (PTR-TOF 8000, Ionicon, Austria).[39]

Car and wood combustion exhausts underwent two different aging scenarios, representing either short aging or medium

Table 1 Overview on combustion and aging experiments with corresponding equivalent photochemical aging days and its average standard deviation during a 4h experiments

Aerosol emission source	No. of samples pooled	Dilution ratio	Equivalent age [d]	Standard deviation of equivalent age [d]
Car, fresh	4	17	0	
Car, short aged	4	17	2.1	1.7
Car, medium aged	4	17	5.0	2.0
Wood stove, fresh	4	60	0	
Wood stove + ESP,[a] fresh	3	60	0	
Wood stove short, aged	4	60	1.4	1.2
Wood stove + ESP,[a] short aged	1	60	2.2	1.5
Wood stove, medium aged	4	60	3.8	2.6

[a] ESP: electrostatic precipitator.

aging in comparison to the maximum atmospheric particle lifetime of two weeks. The atmospheric ages of gasoline car emissions were equivalent to 2.1 or 5 days (based harmonic mean decay of d9-butanol during a 4h experiments) of photochemical OH exposure in the atmosphere assuming an average ambient concentration of OH radicals of 1.5×10^6 cm^{-3}. For residential wood combustion emissions, the average ages were 1.4 or 3.8 equivalent days for the short and medium aging, respectively. Arithmetic means and average standard deviations of the OH exposures during each experiment type are given in Table 1. OH_{exp} reached in the PEAR is sensitive to the input of OH reactive components, which consume the available radicals.[40] For both sources, the transient nature of the exhausts led to natural variance in the rate of exposures to OH (Fig. S1†). Similarly, there was notable variance in the ratio of photolysis to OH exposure (Fig. S2†) and in the consequent reaction pathways of the peroxy radicals (RO_2) formed in the first step of photochemical reactions.[41] Thus, a range of aging conditions is represented in each pooled sample.

The ratio of UVC photolysis to OH_{exp} ($F_{254,exp}/OH_{exp}$) was significantly higher than in the atmosphere, leading to enhanced photolysis of organics and limited RO_2 isomerization compared to atmospheric conditions. However, for most of the operation time the $F_{254,exp}/OH_{exp}$ remained below the limit of 1×10^7 cm s^{-1}, which can be considered the upper limit in regard of atmospheric relevant oxidative flow reaction operation (Fig. S2†).[42]

The fates of low-volatile organic compounds (LVOC) in the PEAR were assessed similarly as in previous studies.[28,43] LVOC lifetime regards to particulate condensation was below 1 s at the PEAR exit (Fig. S3†), based on the particulate condensation sink calculated from the particle number size distributions measured after the PEAR by a Scanning Mobility Particle Sizer (SMPS Classifier Model 3080, DMA model 3081, CPC 3776, TSI). Consequently, the LVOCs condensed onto the particles during the 64 s PEAR residence time in all experiments.

2.2. Filter extraction and ultrahigh resolution mass spectrometry

For filter extraction, filter samples from repetitions of the same experimental conditions were pooled and extracted together to minimize effects of experimental variation (Table 1). For each experimental condition, in total eight 10 mm punches were taken from replicate filters, representing 0.5 m^3 aged or 1 m^3 fresh diluted exhaust gas and placed in a pre-baked glass vial. A mixture (1/1 v%) of methanol (LC-MS grade) and dichloromethane (LC-MS grade) was added to the vial and it was placed in an ice-chilled ultrasonic bath for 30 min. After a final filtration step (0.2 μm PTFE membrane, Sartorius, Goettingen, Germany), the extracts were kept at −25 °C until further analysis.

Direct-infusion electrospray ionization (ESI) Fourier-transform ion cyclotron resonance mass spectrometry (FT-ICR MS) was carried out on a SolariX MRMS platform (Bruker Daltonik, Bremen, Germany) equipped with a 7 T superconducting magnet and an Infinity Cell. All samples were analyzed by electrospray ionization in positive (ESI+) and negative mode (ESI−) as well as atmospheric pressure photoionization in positive mode (APPI). The parameters of the FT-ICR were similar to previous experiments and are described in detail elsewhere.[44] Briefly, for APPI experiments (Kr discharge lamp, 10/10.6 eV) the flow rate was set to 600 μL h^{-1} with a vaporizer temperature of 350 °C. For ESI experiments the spray voltage was set to −/+ 3.5 kV with 1.4 bar nebulizer gas and a flow rate of 200/300 μL h^{-1} for positive and negative mode, respectively. For all ionization techniques, 200 scans were collected in the range of m/z 150–1000 with a resulting mass accuracy below 1 ppm, root-mean square error (RMSE) between 0.15–0.4 ppm and a resolving power >310 000 at m/z 400.

2.3. Data analysis in FT-ICR MS

After internal calibration based on known homologue series of CHO compounds, the mass spectra were exported and further processed by self-written MATLAB algorithms and routines combined in the graphical user interface CERES Processing. The following restrictions were set for the elemental composition assignment: $C_cH_hN_nO_oS_sNa_{na}$, $5 \leq c \leq 100$, $5 \leq h \leq 200$, $n \leq 4$, $o \leq 20$, $s \leq 1$ (ESI+: na ≤ 1, s = 0). Additional limitations were set for H/C ratio (0.4–2.4), O/C ratio (0–1.4), and double bond equivalents (DBE; 0–28). The minimum number of compounds in a compound class was set to five. An intensity based blank removal was used to remove any signals of contaminations originating from the filter sampling, extraction procedure, or

ionization source. Equations used for the calculation of molecular properties: double bond equivalent (DBE), modified aromaticity index (AI_{mod}) and saturation vapor pressure ($\log(C^*)$) as well as definitions for the organic compound volatility ranges are given in Section S1.†

3. Results and discussion

3.1. Compositions of fresh and aged residential wood combustion emissions

Fresh wood combustion emissions already contain oxygen-containing functional groups originating from the incomplete combustion of mainly oxygen-containing biomass constituents like lignin, cellulose, or hemicellulose.[14] Atmospheric aging distinctly shifts the oxygen number distribution towards a broader distribution with higher maximum and average oxygen numbers (Fig. 1a–c), visible in all three ionization techniques. Comparing short and medium aging experiments, the prolonged equivalent age increases the average oxygen number by two (Table S4†), which is higher than the observed increase by one between fresh and short aging.

The photochemical aging of residential wood combustion emissions, on a compound class level, results in a reduction of the number of hydrocarbons (CH) and reduced nitrogen-containing compounds (CHN), because of oxygen addition to the carbon backbone in functional groups (Table S2 and Fig. S4a†), such as alcohol, carbonyl, or nitro group, supported by increasing abundance of oxygen-containing compound classes (CHO, CHNO) in all ionization techniques. Sulfur-containing species are detected in fresh wood combustion

emissions (CHOS), and further increase with atmospheric aging due to secondary reactions with NO_X or SO_X.[45,46] Atmospheric aging also leads to the formation of a new class of CHNOS compounds. However, sulfur-containing compounds are over-represented in the mass spectra due to particularly high sensitivity by ionization in negative mode ESI.[47] The chemical complexity of the organic aerosol increased with additional atmospheric aging, which can be observed in the mass spectra of each dataset (Fig. S5†). The mass spectrometric pattern changed from a lower number of distinct, higher intensity peaks to a more continuous distribution of peaks in a homolog series, with a broader range of oxygenation (e.g., $C_{14}H_8O_6$–$C_{21}H_{22}O_6$: e.g., hydroxylated-anthraquinone like) and higher number of oxidized nitrogen-containing compounds (e.g., $C_{10}H_9N_1O_6$–$C_{18}H_{25}N_1O_6$: e.g., nitro-phthalate like).

Short photochemical aging equivalent to 1.4 days significantly increases the average O/C ratio (ΔO/C: 0.10 (APPI), 0.11 (ESI+), 0.33 (ESI−)) compared to fresh emissions. Enhancement of aging from short to medium causes similar differences in the average O/C ratio for APPI and ESI+ (ΔO/C: 0.07 and 0.11, respectively) as the initial aging step, while for ESI− the increase is lower (ΔO/C: 0.13). The selectivity of each ionization technique for certain compound classes explains this effect. While APPI is selective for non- and low-polar compounds, preferably containing unsaturated structures, e.g., aromatic rings, and ESI+ is selective for polar compounds with basic moieties, ESI− is selective for polar compounds with acidic functional groups, e.g., carboxyl-, sulfate- or nitro-groups.

The number of nitrogen-containing compounds in the fresh wood combustion exhaust was minor. Both short and medium aging show a much higher number of nitrogen-containing compounds compared to the fresh emissions due to the abundant NO_X taking part in the aging reactions in the PEAR (Fig. S4†). The addition of nitrogen during atmospheric aging, e.g., as nitro or nitrate moieties, has been frequently observed and discussed in literature, with ozone-based photochemical oxidation conditions applied in this experiment, enabling pathways that readily form multifunctional organic nitrates ($RONO_2$).[48–50] The less polar compounds detected by APPI show an expected trend, as the nitrogen abundance increases with more intense photochemical aging, while the polar compounds detected by ESI show a different behavior. Especially in ESI−, the number and the total intensity of nitrogen-containing compounds is higher in short-aged wood combustion emissions than in medium-aged emissions. Atmospheric aging leads to the degradation of organic compounds, e.g., due to photo-oxidation, with some compounds being more sensitive to this degradation than others. This is likely reflected by the selectivity of ESI− for acidic and nitrogen-containing compounds (e.g., nitrophenols), that seem to be more efficiently oxidized during prolonged photochemical aging, than other compound classes.[51] This trend is also seen in the total number and total intensity of detected compounds by ESI−, which is not increasing but slightly decreasing for medium aged wood combustion emissions (short aged: number (n) = 2614/total ion current (TIC) = 1.7×10^{10}, medium aged: n = 2050/TIC = 1.2×10^{10}, Table S3†).
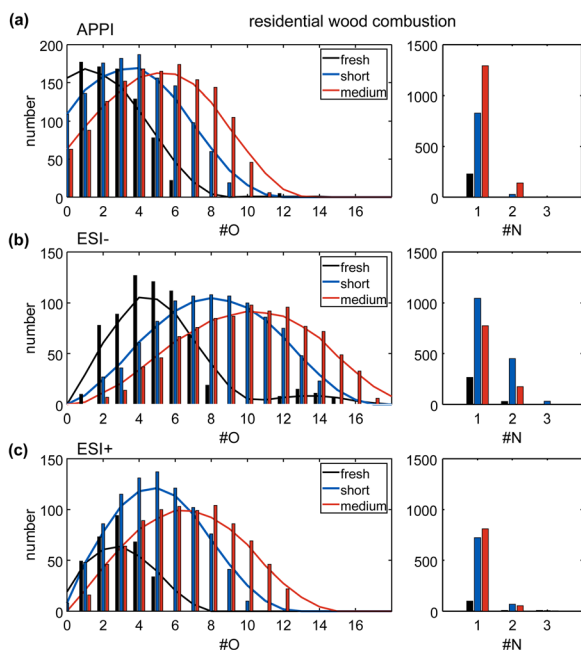

Fig. 1 Number distributions of oxygen (left) and nitrogen (right) in fresh (black), short aged (blue), and medium aged (red) residential wood combustion emissions for each ionization technique (a: APPI, b: ESI−, c: ESI+).
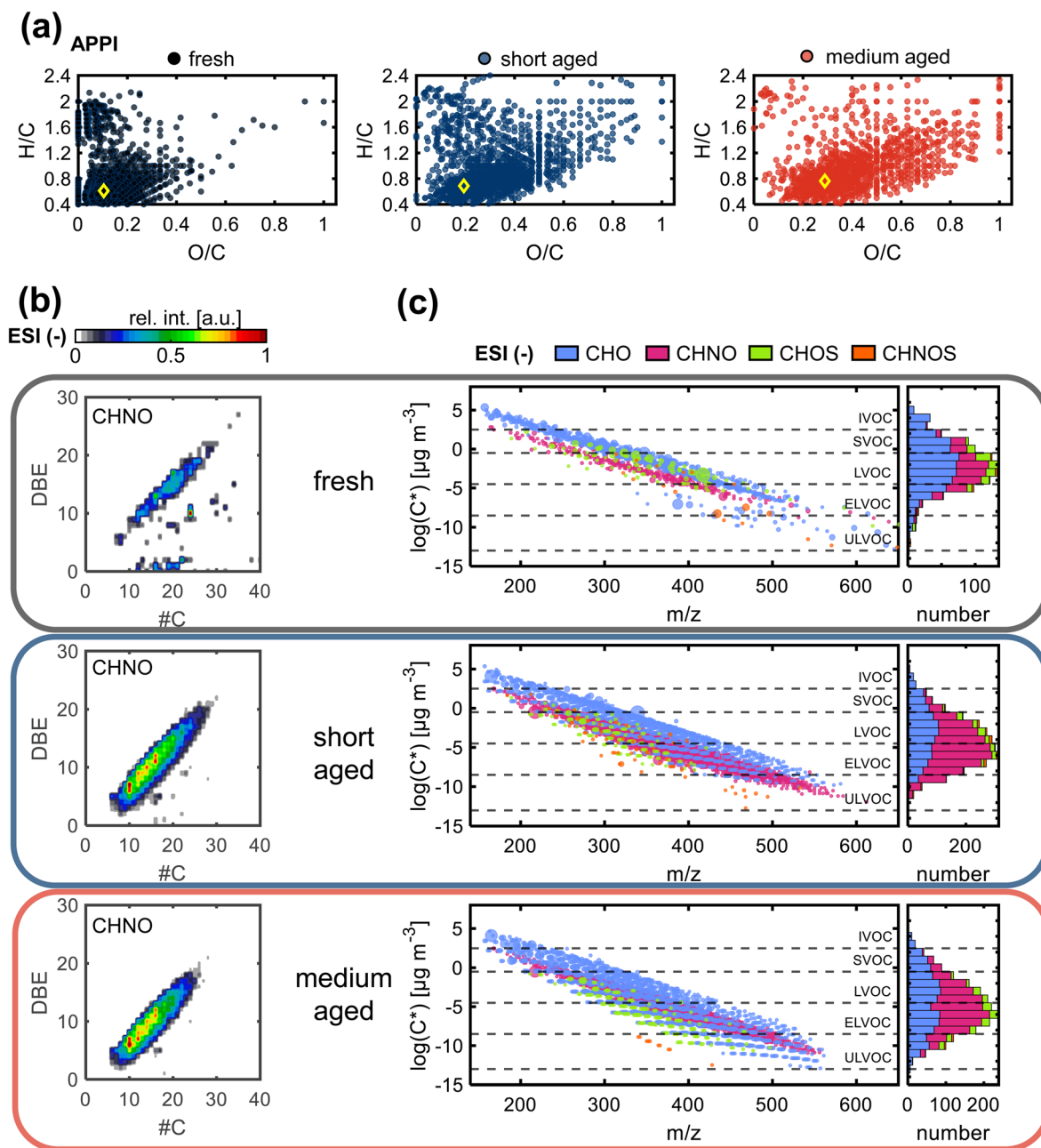
Fig. 2 (a) Van Krevelen diagrams of residential wood combustion emissions APPI results with fresh organic aerosol (left) indicated in black, compounds newly formed during short aging (center) indicated in blue and compounds uniquely formed during medium aging (right) displayed in red. Intensity-weighted average H/C and O/C ratios of each dataset are indicated by yellow bordered diamonds. (b) Double bond equivalent (DBE) *versus* carbon number contour plots of the summed CHNO compound class in fresh, short aged and medium aged ESI− data of residential wood combustion emissions. (c) Calculated saturation vapor pressure ($\log(C^*)$) *versus* m/z ratio plots of assigned elemental compositions (ESI−) with indicated compounds class (color) and relative intensity (dot size) and histogram of $\log(C^*)$ distribution. Organic compound volatility ranges of intermediate-volatile (IVOC), semivolatile (SVOC), low-volatile (LVOC), extremely-low volatile (ELVOC) and ultra-low volatile (ULVOC) are indicated by dotted horizontal lines.

The observed increase in O/C ratio as well as the decrease in H/C ratio by photochemical aging are linked to decreasing aromaticity and increased functionality (Fig. 2a, S6, and Table S4†). For wood combustion emissions, the average AI_{mod} is steadily decreasing with increasing equivalent photochemical age, likely due to ring-opening reactions. The general chemical space of compounds that are newly formed during medium aging is mostly overlapping with compounds that are already formed after short aging, with a small shift towards higher O/C ratios with higher photochemical exposure. Still, the difference in O/C and AI_{mod} between fresh to short aging is larger than from short to medium aging despite the equidistance in age of

approximately 1.5 days. The formation of highly oxidized, partially aromatic compounds, is best observed in ESI− (Fig. S6b†) and is expected in the formation of SOA from PAHs.[52,53] In general, SOA formation by homogenous oxidation and consequent condensation of the gas phase organics is dominating at the beginning of atmospheric aging, being the faster reaction compared to heterogenous oxidation of the particle phase that becomes more relevant with increasing aging duration.

The contour plot of DBE versus carbon number (Fig. 2b) for all compounds in the CHNO class (ESI−) summarizes the previously discussed trends. CHNO compounds with aromatic rings are an important constituent of BrC due to their potentially strong light-absorbing properties.[54,55] Fresh emissions contain the lowest number of CHNO compounds, with a narrow elliptical distribution from 10–30 carbon atoms and DBE 5–23 as well as some dispersed signals and unsaturated species, likely fatty acids. After short aging, only the elliptical distribution remains, but it is shifted to lower DBE values, while at the same time getting broader, as a result of the formation of compounds with higher degree of alkylation. After medium aging, the main elliptical distribution remains mostly the same, but slightly shrinks at the high DBE end, which is explained by photodegradation.[56] The same trend is observed for the CHO and CHOS compound classes (Fig. S7†). Similarly, compounds formed during the step from short to medium aging show elliptical distribution patterns that are already observed after short aging, including the main CHON and CHO compound classes, as well as minor contributions of CHOS (Fig. 2b, and S7†). Notably, for all compounds classes, most of the species detected after medium aging (3.8 days) are already detected after short aging (1.4 days), with the compounds occupying the same chemical space, especially for polar organic aerosol constituents. In ESI− and ESI+ only 22% and 35% of the assigned elemental compositions in medium aged wood combustion emissions are uniquely formed after medium aging, respectively, while most compounds are already identified in the short aging sample (77% and 64%, respectively). The decline in the formation rate of new elemental compositions is a result of counteracting mechanisms that, on the one hand, form new compounds due to atmospheric oxidizing agents and, on the other hand, degrade compounds via photooxidation that leads to the formation of smaller products that are too volatile for filter sampling or fall below the lower limit of the accessible m/z range.

The formation of higher molecular weight secondary organic compounds during photochemical aging, either due to functionalization, radical recombination, or oligomerization reactions, is necessarily accompanied by a reduction of the volatility of product compounds.[57] Fresh wood combustion emissions contain mainly semi- or low-volatile organic compounds (SVOC, LVOC), which during atmospheric aging are forming new LVOC (Fig. 2c), extremely-low volatile organic compounds (ELVOC) and even ultra-low volatile organic compounds (ULVOC). As discussed before, this is mainly a result of oxidation reactions, also including the addition of nitrogen-containing functional groups, as well as a higher degree of alkylation, which is

highlighted by the width of the striped pattern of the CHO class in the long-aged wood combustion emission (Fig. 2c). Each CHO class band consists of compounds with the same oxygen number. Compounds with higher oxygen number and lower volatility are formed after medium aging, compared to short aging. Comparing short and medium aged emissions, an increase of CHOS compounds is observed in the LVOC to ULVOC region after medium aging. These secondary reaction products have O/S ≥ 4, which is an indicator for organic sulfate, a main product of reactions with SO_2. The very low volatility of the organic sulfates means they are predominately partitioned to the condensed phase of particles, where they impact the ability to act as cloud condensation nuclei due to their high hygroscopicity.[58,59] The observed low-volatility CHON compounds have a very high average O/N ratio of 7.7 after short aging and 9.3 after medium aging. A variety of nitrogen-containing functional groups as well as the combination with oxygen-containing functional groups are known to result from secondary aging reactions, e.g., nitro, nitro-phenols, organic nitrates, acyl peroxyl nitrates and unsaturated hydroxy nitrates.[60,61] These structural modifications of CHNO compounds can determine the light-absorption properties of aerosols, especially in the UV to visible light wavelength range, and therefore have a significant impact on the direct radiative forcing properties of the aerosols.[54,55]

3.2. Effect of an electrostatic precipitator on the PM composition

The ESP removed parts of the primary particles, leaving a reduced number of particles as well as the mostly unaffected volatile primary emission for SOA formation.[36] In the comparison of the mass spectra between fresh and short aged emissions from the wood stove with and without ESP, no major difference could be found (Fig. S8†). Therefore, the ESP mostly has a quantitative, but not a strong qualitative effect on particulate emissions.

One minor difference between the experiments with and without an ESP is the higher number of oxygenated compounds (CHO, CHNO, CHNOS, CHOS) that were detected at low intensities in the samples with ESP, either uniquely or even in common with emissions that have undergone short aging. The observation of these compounds may be a result of the higher ratio of oxidants to particles, as well as the formation of ozone from the ESP that may have resulted in minor aging of the fresh wood stove emissions.[62] However, there were no strong differences in the observed mass spectrometric patterns of fresh emissions. Van Krevelen diagrams of the respective datasets (Fig. S9†) show that, for fresh and short aged experiments with and without ESP, unique elemental compositions are found in a similar chemical space (medium to high O/C, medium to low H/C). The strong similarity of the fresh and aged wood combustion emissions with and without the implementation of an ESP is demonstrated also by the similarity in the averages and distribution of values in volatility and carbon oxidation states (Fig. S10†).

During the single short aging experiment with ESP, the ESP had lower particle reduction efficiency than given by Brunner *et al.*[36] However, no quantitative effect on the aging is investigated here and the similar chemical composition of the short-aged aerosol meets the expected outcome from a similar composition of the fresh emissions.

Fig. S9† shows an upset plot of the comparison of short aged wood combustion emissions with and without application of the ESP for short aging. Most elemental compositions in ESI− ($n = 2210$) were detected regardless of the ESP, with only a small number of compounds detected uniquely without an ESP ($n = 400$) or with an ESP ($n = 487$). A similar effect is observed with the other ionization techniques (Fig. S9†). The lower number of particles in the primary aerosol after the ESP appears to not affect the composition of secondary organic aerosol compounds formed during the photochemical aging of wood combustion emissions, although the TIC of detected compounds is generally reduced, *e.g.*, in APPI roughly halved (TIC APPI short aging, without ESP: 2.15×10^{10}, with ESP: 9.99×10^{9}). It should be noted that atmospheric pressure ionization techniques are not necessarily quantitative and detected intensities may vary largely due to ion suppression effects, especially in electrospray ionization, but, to a lower extent, also in APPI.[63]

3.3. Composition of fresh and aged gasoline car emissions

Only few hundred compounds could be detected from the fresh gasoline car emissions. These compounds are low in intensity and predominately in the CHO class, with minor numbers of CH, CHN, CHNO and CHOS species (Tables S2 and S3†). This reflects the effective removal of primary particles by the efficient combustion of commercial gasoline in the engine, combined with exhaust gas cleaning by the in modern three-way catalytic converter and GPF.[10,37]

Nevertheless, VOCs and inorganic gases, such as NO_x and for modern cars particularly NH_3, act as precursors for secondary particles and consequently contribute to the PM2.5 burden.[64,65] The oxygen number distribution (Fig. 3a–c) shows a large shift from fresh to short aged emissions in all ionization techniques, regarding the observed number of compounds, as well as the intensity-weighted average number of oxygen atoms and the summed intensity of assigned signals (Table S4†). For both ESI polarities, the maximum of the distribution is shifted by a factor of more than two from fresh to short aged emissions. For APPI and ESI− the step from short to medium aging is a continuation of the increase in oxygen content observed in the step from fresh to short aging, but with a lower increase of oxygenation. In contrast, ESI+ shows the opposite effect, with the oxygen number distribution shifting back to a similar range already observed for fresh car emissions. To explain this effect, it must be considered that most detected oxygen-containing compounds after short aging of car emissions also contain up to three nitrogen atoms. Nitrogen-containing compounds, detected in ESI+, were predominantly formed during short aging, but some CHON were already degraded after medium photochemical aging (Fig. S11†). As this degradation of CHON compounds is not observed in ESI− and APPI data, neither in the oxygen nor in the nitrogen number distribution, the selectivity of ESI+ must play a key role for the identification of responsible structural features. ESI+ is selective for basic functional groups, *e.g.*, amine, amides, basic aromatic rings (pyridine, quinoline). Nitrogen-containing compounds detected after short aging have a low average aromaticity (average AI_{mod} = 0.06) (Fig. 4a and b). Therefore, short aging most likely produces amine or amide functionalities that are consequently degraded if the photochemical exposure is extended to the medium level (number of CHNO + CHN: fresh: 217, short: 1333, medium: 452).

In ESI− and APPI the number of nitrogen-containing species is drastically increased after short aging and even further increased after medium aging, with up to four nitrogen atoms per molecule. These nitrogen-containing compounds are likely a result of the high NH_3 and NO_x content of the emissions. Notably, the average O/N ratio remains the same after short or medium aging (APPI: 4.1 ESI−: 6.5) as both the average nitrogen and the average oxygen number are likewise increased (Table S3†).

Therefore, the secondary reactions leading to the formation of these compounds seem to continue constantly for the full exposure range of the experiment. The matching addition of oxygen and nitrogen functionalities can be driven, for example, by the combination of OH-radical-initiated oxidation and ammonia-driven carbonyl-to-imine conversion.[66] This also enables radical recombination and condensation reactions that increase the carbon number of the aged PM. The number, intensity, DBE, and carbon number are all continuously increased from fresh to short and medium aged emissions for the CHON and the CHO compound class, with the effects highlighted in the DBE *versus* carbon number plots (Fig. 4b, and S7a†).
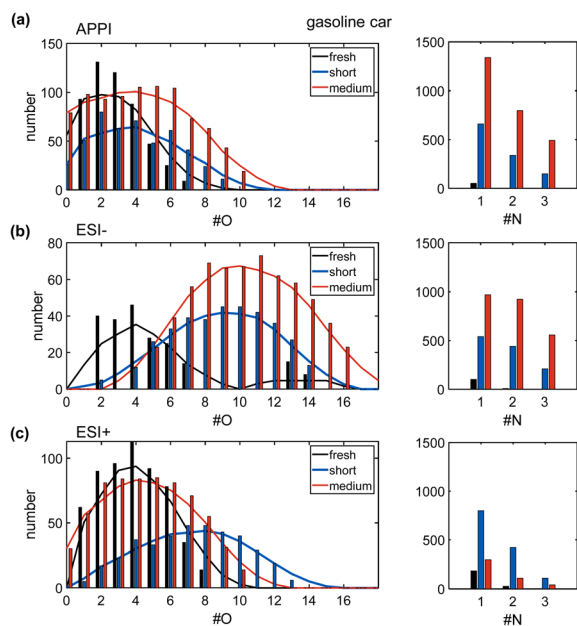

Fig. 3 Number distribution of oxygen (left) and nitrogen (right) in fresh (black), short aged (blue) and medium aged (red) gasoline car emissions for each ionization technique (a: APPI, b: ESI−, c: ESI+).
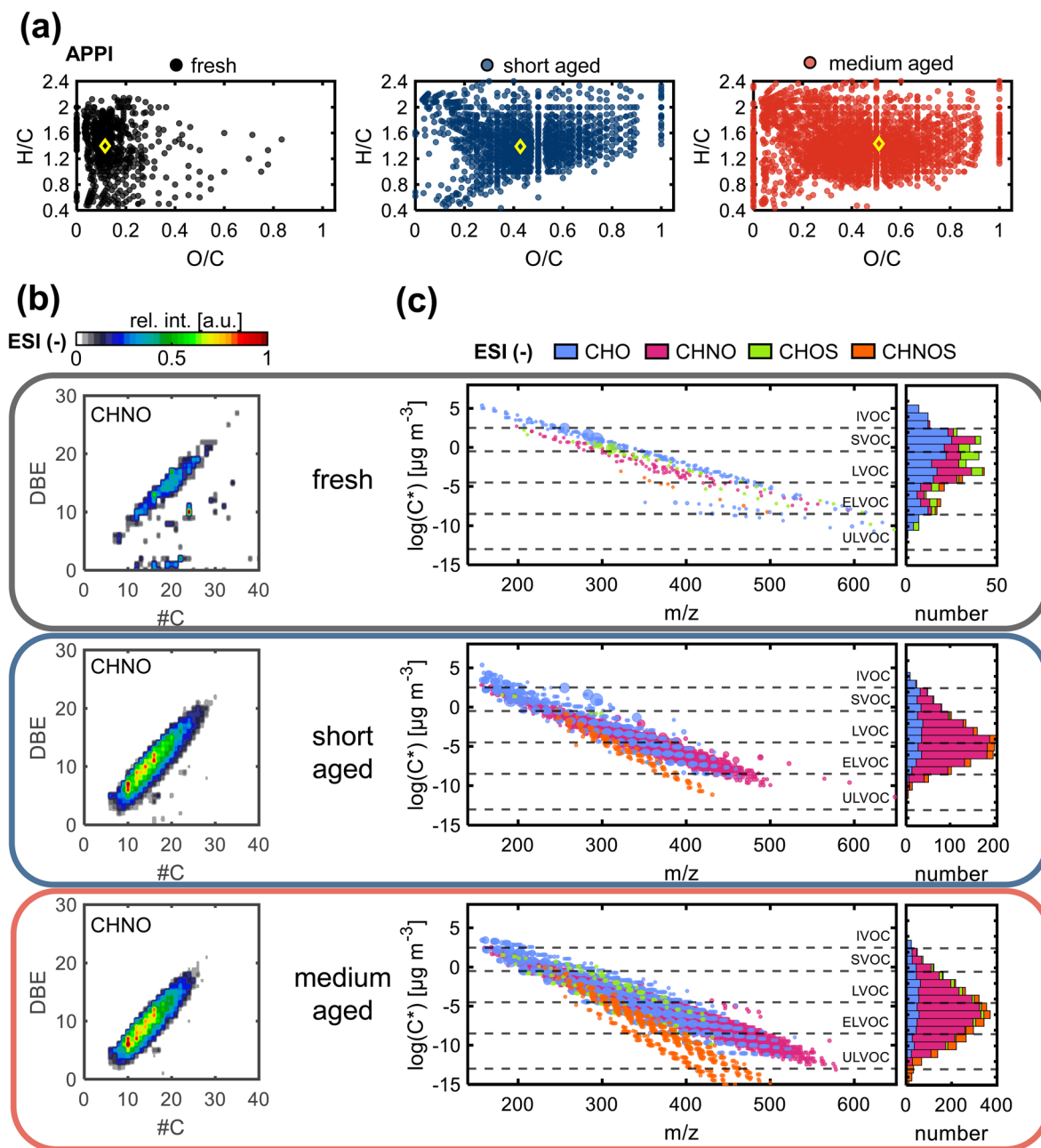
Fig. 4 (a) Van Krevelen diagrams of gasoline car emissions (APPI) data with fresh organic aerosol (left) indicated in black, compounds newly formed during short aging (center) indicated in blue and compounds uniquely formed during medium aging (right) displayed in red. Intensity-weighted average H/C and O/C ratios of each dataset are indicated by yellow bordered diamonds. (b) Double bond equivalent (DBE) *versus* carbon number contour plots of the summed CHNO compound class in fresh, short aged and medium aged ESI− data of residential wood combustion emissions. (c) Calculated saturation vapor pressure (log($C*$)) *versus* m/z ratio plots of assigned elemental compositions (ESI−) with indicated compounds class (color) and relative intensity (dot size) and histogram of log($C*$) distribution. Organic compound volatility ranges of intermediatevolatile (IVOC), semivolatile (SVOC), low-volatile (LVOC) extremely-low volatile (ELVOC) and ultra-low volatile (ULVOC) are indicated by dotted horizontal lines.

Fresh gasoline car emissions only contain a minor number of CHOS compounds ($n = 46$) and CHNOS compounds ($n = 9$) (Fig. S13a†). Due to the presence of NH_3 and NO_x in addition to SO_2 in the emissions, after short aging, CHOS compounds remain rare, while a small number of CHNOS compounds ($n = 109$) is newly formed with high DBE values (DBE > 10) and likely

containing at least one aromatic ring (average $AI_{mod} = 0.62$) (Fig. S13b†). With higher photochemical ages, even more CHNOS compounds, but also CHOS compounds are formed, not only with aromatic structures but also in a second region at lower DBE values reducing the average AI_{mod} of CHNOS compounds to 0.44. CHOS compounds show almost the same

distribution in the DBE *versus* carbon number plot after medium aging but, with two separate regions at low and high DBE values but a lower average AI_{mod} of 0.25. The CHOS compounds only formed after medium aging may be degradation products of CHNOS compounds, which undergo photochemical degradation reactions leading to ring-opening and the loss of DBE or rather aromaticity as well as nitrogen moieties. The aromatic as well as aliphatic sulfur-containing compounds are known for their hygroscopicity that modifies the ability of the aerosol particle to act as cloud condensation nuclei,[59] as well as the induction of adverse health effects and oxidative stress, especially by aromatic sulfur-containing species.[67]

After medium aging, the main fractions are the uniquely identified compounds (APPI: 59%, ESI−: 56%, ESI+: 83%, compared to short aging PM) followed by the fraction of compounds that are common in short and medium aged PM (Fig. S11†). Compounds only formed after medium aging also display a lower volatility compared to compounds formed after short aging (Fig. 4c), enforcing the previously observed pattern created from compounds after short aging in the direction of lower volatility and higher molecular weight in comparison to fresh exhaust.[68]

3.4. Comparison of car and wood combustion emission aging

The laboratory aging of two anthropogenic aerosol emission sources representing current modern technologies highlights the complex dependencies of secondary PM formation and composition on the emitted primary organic aerosol composition and concentration. When comparing the effect of atmospheric aging on car and residential wood combustion, both emission types lead to the formation of a broad variety of oxidized organic compounds and the molecular complexity increases with ongoing photochemical aging. Increasing aging duration enhances the average carbon oxidation state (OS_C) while decreasing the average volatility of OC (Fig. S10†).

Fresh residential wood combustion emissions contain already a high number of low-volatile organic compounds from incomplete thermal degradation of the biomass, while primary gasoline car emissions contain only a minor number of detectable compounds due to the efficient combustion of fuel and the application of particle filters. During laboratory photochemical aging both emission types undergo intense photooxidation, adding oxygen- as well as nitrogen- and sulfur-containing moieties to the primary organic aerosol, and forming new compounds with higher O/C ratio (Fig. 2a and 4a). This also results in a shift towards lower volatility which can be observed for all compound classes alike (Fig. 2c and 4c). Interestingly, both emissions show the same evolution in the Van Krevelen space by keeping H/C of the fresh emissions and increasing O/C. This corresponds to the addition of alcohol (–OH) or peroxide moieties (–OOH).[69] Since APPI is particularly sensitive for aromatic compounds, we may infer functionalization of aromatic hydrocarbons as well as further oxidation of oxygenated hydrocarbons without fragmentation. While this behavior is similar in ESI+ and ESI− for wood combustion

emissions, aged gasoline car emissions show a decreasing slope of −1 in the Van Krevelen space in ESI−; in ESI+, no slope can be obtained because of a decreasing O/C from short to medium aging. This untypical observation may be a consequence of fragmentation reactions leading to the loss of nitrogen (Table S3†), which is co-abundant with oxygen in *e.g.*, nitro groups or organic nitrates. When combining the average carbon oxidation state (OS_C) with the volatility (Fig. S10†), the center of the distribution (intensity weighted average) is shifted towards the top left of the diagram, indicating higher average oxidation and lower volatility with increasing aging intensity.

3.4.1. CHNO compounds. In contrast to the similar increase in the oxygen number distribution for both emission types the nitrogen number distribution is clearly elevated in the aged car emissions compared to wood combustion. This is due to the emission of NH_3 and NO_x, which enhances both the total number of CHON compounds as well as the average number of nitrogen atoms per molecule (Fig. 3). In comparison to the aging of wood combustion emissions, the medium aging of gasoline car emissions shows a smaller preservation of compounds, that were present after short aging (Fig. S7 and S11†). More unique compounds are identified after medium aging, indicating a higher chemical conversion than wood combustion emissions at comparable exposure to OH radicals. For both emission types, ESI data shows a deviation from this trend, with nitrogen numbers peaking after short aging and then decreasing (ESI−) or remaining constant (ESI+) after medium aging. The decreasing trend in abundance may be explained by photodegradation of labile CHNO compounds, *e.g.*, nitrophenols,[28] which are in the case of the gasoline car, preferably ionized by ESI+ and in the case of the wood combustion preferably ionized by ESI−. As both polarities are selective for different types of compounds, the functional groups formed during short aging of the two emission sources must be different, with short aged gasoline car emissions containing rather basic nitrogen moieties and short aged wood combustion emissions containing more acidic nitrogen moieties.

The concentrations of NH_3 and NO_X dictates the prevalent atmospheric aging mechanism, as due to their higher levels in the fresh emissions from the gasoline car, the number of nitrogen-containing compounds is higher. CHNO compounds can have distinct effects on the light-absorbing properties of the aerosol due to the chromophore character of these compounds, *e.g.*, in combination with aromatic ring structures as nitro-aromatics.[70] Furthermore, aged wood combustion emissions contain a larger share of aromatic as well as condensed aromatic ring structures than car engine emissions (Table 2). In both cases, the absolute number of aromatic compounds is increased during short as well as medium aging, but the relative number is steady or decreasing. While the increase in total compound number from car emissions is higher compared to wood emissions, mostly aliphatic or partially unsaturated compounds are formed during photochemical aging and the increase of highly aromatic compounds is limited (Fig. 4b), in contrast to the aging of wood combustion emissions where secondary compounds largely remain aromatic (Fig. 2b).

Table 2 Relative number of assigned elemental compositions in each modified aromaticity index (AI_{mod}) bin of gasoline car and residential wood combustion emissions in APPI data. $AI_{mod} > 0.5$ indicates aromatic structures and $AI_{mod} > 0.67$ indicates condensed aromatic structures

Type	Aging	Rel. number (abs. number) AI_{mod} bins			
		$0 \leq 0.25$	$0.25 \leq 0.5$	$0.5 \leq 0.67$	$0.67 \leq 1$
Car	Fresh	0.48 (295)	0.34 (213)	0.08 (50)	0.10 (62)
	Short	0.63 (1027)	0.25 (411)	0.06 (101)	0.06 (98)
	Medium	0.64 (2409)	0.26 (965)	0.08 (310)	0.03 (100)
Wood	Fresh	0.16 (180)	0.11 (123)	0.17 (194)	0.56 (638)
	Short	0.18 (374)	0.15 (326)	0.25 (525)	0.42 (902)
	Medium	0.17 (493)	0.18 (517)	0.29 (814)	0.35 (1000)

Regarding the volatility of aged organic compounds, species from car emissions decrease in volatility with increasing photochemical aging and more extremely-low volatile organic compounds are formed, while wood combustion emissions remain at a similar level of low volatility (Fig. 2c, 4c and S12†). However, it should be mentioned that the applied analysis is covering the extracted fraction of PM2.5 and, gas-phase volatile compounds will be discussed in future studies. As wood is a complex biopolymer with, *e.g.*, large cellulose or lignin macromolecules, higher molecular weight compounds can be emitted by incomplete combustion of the biomass. In contrast, the constituents of gasoline fuel are low molecular weight and SOA formation during atmospheric aging has to start from smaller molecular building blocks to form heavier, less volatile species.

3.4.2. Sulfur-containing compounds. Negative mode electrospray ionization reveals the distinct formation of oxidized sulfur-containing compounds, some also containing nitrogen, during atmospheric aging of both, gasoline car and residential wood combustion emission. ESI− is especially sensitive for the ionization and detection of these compounds, due to the acidity of most sulfur-containing functional groups, therefore the observed signal intensity does not reflect the actual trace amounts of these compounds. CHOS and CHNOS compounds are well known as secondary atmospheric aging products forming in the condensed phase of acidic sulfate seeds or by reactions of SO_2 with carboxylic acids.[46,71,72] They are often identified as a major fraction in atmospheric aerosol samples, especially under the influence of anthropogenic emissions.[73,74] SO_2 is emitted in traces from the engine in gasoline cars and originates mainly from the lubrication oil. Wood combustion likewise releases traces of SO_2 from the thermal degradation of sulfur-containing biomass constituents like amino acids or disulfide-bonds.[75] Also, small amounts of CHOS compounds may be emitted directly due to incomplete combustion of these biomass constituents.

During the aging of emissions, CHOS compounds are, to a minor extent, formed after short aging as well as medium aging of wood combustion emissions, but for car emissions they are only formed after medium aging (Fig. S7†). In contrast, CHNOS compounds in wood combustion emissions are only

formed after short aging but are almost vanished after medium aging, while for car emissions they are continuously formed after short and medium aging. In the case of wood combustion emissions, CHNOS compounds seem to face the same fate as other nitrogen-containing compounds of the same source, that degrade with ongoing photochemical aging, comparable to a consecutive first-order reaction. In gasoline car emissions most sulfur-containing compounds only appear after prolonged aging, as they are predominately formed by secondary reactions with SO_2.

3.4.3. Primary emission fingerprints in aged emissions. Primary organic aerosol emissions contain distinct molecular markers that are used for identification in ambient atmospheric studies, *e.g.*, for source apportionment.[76] Moreover, also markers for aged emissions, such as 2,3-dihydroxy-4-oxopentanoic acid (DHOPA) for toluene photooxidation, have been established.[77] Photochemical aging generated unique aged emission marker molecules while, on the contrary, increasing the number of common oxidation compounds that are produced by secondary aging reactions regardless of the combustion emission source. The similarity of elemental compositions detected in short and medium aging of gasoline car and residential wood combustion emissions (Fig. S14†) reveals an increase in both, the emission-unique compounds, and the emission-common compounds. Extensive atmospheric aging, *e.g.*, during long-range transport of mixed emission sources from anthropogenic, biogenic and wildfires emissions, has been observed to result in the formation of a heavily oxidized mixture of organic aerosol compounds that could no longer be clearly assigned to one emission source.[61] Notably, the number of detected compounds common to the two emission sources is, in this study, always lower than the number of emission-unique compounds (*e.g.*, short aging: unique wood: 1486/unique car: 996/common: 641) but the relative intensity that is represented by the common elemental compositions is always around 50% of the total intensity. This is also reflected by the change of molecular properties during aging (Fig. 2a–c and 4a–c), that are consequently also responsible for properties of the PM itself, for example, the light absorption, the hygroscopicity, and the ability of the particles to act as cloud condensation nuclei. Eventually, short, and medium aging alters the molecular fingerprints to oxidized organic species but maintains some compositional differences between the two aerosol emission sources. Fresh emission constituents are still present in aged emissions, but with lower relative intensity. Extrapolating these findings toward the upper limit of atmospheric particle residence, a further reduction in fresh emission markers and a higher similarity in chemical composition can be expected.

The two exhaust aftertreatment technologies had different effects of the composition of the aged emissions. While the GPF virtually removed the total PM2.5 from the emissions, the ESP only decreased the released amount of PM2.5. Therefore, secondary PM2.5 formed during photochemical aging of car emissions exclusively result from gas-to-particle conversion, implying a substantial oxidation to lower the vapor pressure of fresh emission constituents to form secondary particles. In

contrast, aged wood combustion emissions still contain a large fraction of primary particulate emissions, which usually exhibit slower oxidation kinetics than homogeneous gas phase oxidation and may even be shielded from extensive photooxidation by the formation of a protective organic layer on the particle (*i.e.*, "shielding effect").[78,79]

However, wood combustion organic aerosol, *i.e.*, biomass burning organic aerosol (BBOA), has a higher OS_C than aerosol from the gasoline car, *i.e.*, hydrocarbon-like organic aerosol. Therefore, after similar equivalent photochemical aging, both types of combustion emissions feature similar bulk properties (Table S4†) but maintain distinct different molecular compositions (Fig. 2 and 4).

4. Conclusions

Applying three complementary ionization techniques of different selectivity (APPI, ESI+, ESI−) combined with ultrahigh resolution mass spectrometry provides molecular insights into the effect of short to medium atmospheric aging on the chemical composition from modern combustion emission sources. Sum formula assignment based on exact masses revealed that photochemical aging produces most of the organic aerosol constituents for both gasoline car and wood combustion emissions already within short photochemical exposure (average of 2.1 and 1.4 equivalent days, respectively). Prolonged photochemical aging leads to the formation of new compounds which are more oxidized with higher nitrogen and sulfur content. In contrast, some nitrogen-containing compounds appear to degrade when the photochemical exposure is enhanced.

In the case of wood combustion emissions, medium atmospheric aging decreases the aromaticity and increases oxygenation, but with only a minor change in volatility, which remains low. The total number of detected compounds increases faster for the aged emissions from the EURO 6 gasoline car from fresh to short and medium aged emissions, as fresh emissions are comprised of gases, but virtually no PM2.5. The increase in oxidated organic aerosol is accompanied by a substantial addition of nitrogen, *e.g.*, as organic nitrates, which likewise increases with the equivalent photochemical age. Furthermore, CHOS and CHNOS compounds are formed during short aging, due to secondary reactions including SO_2. SO_2 is formed during the combustion from sulfur-containing species in the fuels and, for the car exhaust, lubrication oil.

The application of an ESP on the wood stove reduces the total intensity of detected compounds, but the chemical composition remains largely unchanged for both, fresh and aged exhausts. Moreover, some primary wood combustion markers in the particle phase survive short and medium photochemical aging, protected from gas phase oxidants by organic particle coating (shielding effect). In contrast, the low amount of detected organic compounds in fresh gasoline car emissions are predominantly semi-volatile species, which are continuously evolving in the exhaust gas flow. Since the particles in the aged car emissions consist exclusively of secondary compounds, traditional markers are not applicable anymore.

Therefore, investigations of the changes in secondary emission formation are required when new combustion or exhaust aftertreatment technology are being implemented on established combustion emissions categories, such as residential wood combustion or traffic emissions.

Author contributions

E. S.: methodology, investigation, formal analysis, writing – original draft, visualization, writing – review & editing; H. C.: conceptualization, formal analysis, supervision, writing – review & editing, project administration; H. J. H., M. I., P. Y., M. S., M. K., J. L., N. G., J. O., Z. F.: investigation, writing – review & editing; A. H.: methodology, investigation, formal analysis, writing – original draft, visualization, writing – review & editing; C. P.: methodology, software, resources, writing – review & editing, supervision; Y. R., O. S., R. Z.: conceptualization, resources, writing – review & editing, funding acquisition.

Conflicts of interest

There are no conflicts of interest to declare.

Acknowledgements

References

1 R. A. Silva, Z. Adelman, M. M. Fry and J. J. West, The Impact of Individual Anthropogenic Emissions Sectors on the Global Burden of Human Mortality due to Ambient Air Pollution, *Environ. Health Perspect.*, 2016, **124**, 1776–1784.

2 H. Orru, H. Olstrup, J. Kukkonen, S. López-Aparicio, D. Segersson, C. Geels, T. Tamm, K. Riikonen, A. Maragkidou, T. Sigsgaard, J. Brandt, H. Grythe and B. Forsberg, Health impacts of PM2.5 originating from residential wood combustion in four nordic cities, *BMC Public Health*, 2022, **22**, 1286.

3 E. F. Choma, J. S. Evans, J. A. Gómez-Ibáñez, Q. Di, J. D. Schwartz, J. K. Hammitt and J. D. Spengler, Health benefits of decreases in on-road transportation emissions in the United States from 2008 to 2017, *Proc. Natl. Acad. Sci. U.S.A.*, 2021, **118**, e2107402118.

4 X. Zhu, Q. Zhang, X. Du, Y. Jiang, Y. Niu, Y. Wei, Y. Zhang, S. N. Chillrud, D. Liang, H. Li, R. Chen, H. Kan and J. Cai,

Respiratory Effects of Traffic-Related Air Pollution: A Randomized, Crossover Analysis of Lung Function, Airway Metabolome, and Biomarkers of Airway Injury, *Environ. Health Perspect.*, 2023, **131**, 57002.

5 N. Paisi, J. Kushta, A. Pozzer, A. Violaris and J. Lelieveld, Health effects of carbonaceous PM2.5 compounds from residential fuel combustion and road transport in Europe, *Sci. Rep.*, 2024, **14**, 1530.

6 I. Stanimirova, D. Q. Rich, A. G. Russell and P. K. Hopke, Common and distinct pollution sources identified from ambient PM2.5 concentrations in two sites of Los Angeles Basin from 2005 to 2019, *Environ. Pollut.*, 2024, **340**, 122817.

7 M. Glasius, A. Hansen, M. Claeys, J. S. Henzing, A. D. Jedynska, A. Kasper-Giebl, M. Kistler, K. Kristensen, J. Martinsson, W. Maenhaut, J. K. Nøjgaard, G. Spindler, K. E. Stenström, E. Swietlicki, S. Szidat, D. Simpson and K. E. Yttri, Composition and sources of carbonaceous aerosols in Northern Europe during winter, *Atmos. Environ.*, 2018, **173**, 127–141.

8 Z. Zhang, J. Gao, L. Zhang, H. Wang, J. Tao, X. Qiu, F. Chai, Y. Li and S. Wang, Observations of biomass burning tracers in PM2.5 at two megacities in North China during 2014 APEC summit, *Atmos. Environ.*, 2017, **169**, 54–64.

9 D. Salameh, J. Pey, C. Bozzetti, I. El Haddad, A. Detournay, A. Sylvestre, F. Canonaco, A. Armengaud, D. Piga, D. Robin, A. Prevot, J.-L. Jaffrezo, H. Wortham and N. Marchand, Sources of PM2.5 at an urban-industrial Mediterranean city, Marseille (France): Application of the ME-2 solver to inorganic and organic markers, *Atmos. Res.*, 2018, **214**, 263–274.

10 A. Joshi and T. V. Johnson, Gasoline Particulate Filters—a Review, *Emiss. Control Sci. Technol.*, 2018, **4**, 219–239.

11 A. Kuye and P. Kumar, A review of the physicochemical characteristics of ultrafine particle emissions from domestic solid fuel combustion during cooking and heating, *Sci. Total Environ.*, 2023, **886**, 163747.

12 J.-H. Tsai, S.-J. Chen, K.-L. Huang, W.-J. Lee, W.-C. Kuo and W.-Y. Lin, Characteristics of particulate emissions from a diesel generator fueled with varying blends of biodiesel and fossil diesel, *J. Environ. Sci. Health, Part A: Toxic/Hazard. Subst. Environ. Eng.*, 2011, **46**, 204–213.

13 P. T. Aakko-Saksa, L. Rantanen-Kolehmainen and E. Skyttä, Ethanol, isobutanol, and biohydrocarbons as gasoline components in relation to gaseous emissions and particulate matter, *Environ. Sci. Technol.*, 2014, **48**, 10489–10496.

14 H. Czech, T. Miersch, J. Orasche, G. Abbaszade, O. Sippula, J. Tissari, B. Michalke, J. Schnelle-Kreis, T. Streibel, J. Jokiniemi and R. Zimmermann, Chemical composition and speciation of particulate organic matter from modern residential small-scale wood combustion appliances, *Sci. Total Environ.*, 2018, **612**, 636–648.

15 H. Khodaei, F. Guzzomi, D. Patiño, B. Rashidian and G. H. Yeoh, Air staging strategies in biomass combustion-gaseous and particulate emission reduction potentials, *Fuel Process. Technol.*, 2017, **157**, 29–41.

16 K. Nuutinen, J. Jokiniemi, O. Sippula, H. Lamberg, J. Sutinen, P. Horttanainen and J. Tissari, Effect of air staging on fine particle, dust and gaseous emissions from masonry heaters, *Biomass Bioenergy*, 2014, **67**, 167–178.

17 H. Lamberg, O. Sippula, J. Tissari and J. Jokiniemi, Effects of Air Staging and Load on Fine-Particle and Gaseous Emissions from a Small-Scale Pellet Boiler, *Energy Fuels*, 2011, **25**, 4952–4960.

18 G. C. Tiao, G. E. P. Box and W. J. Hamming, Analysis of Los Angeles Photochemical Smog Data: A Statistical Overview, *J. Air Pollut. Control Assoc.*, 1975, **25**, 260–268.

19 T. Castro, S. Madronich, S. Rivale, A. Muhlia and B. Mar, The influence of aerosols on photochemical smog in Mexico City, *Atmos. Environ.*, 2001, **35**, 1765–1772.

20 R.-J. Huang, Y. Zhang, C. Bozzetti, K.-F. Ho, J.-J. Cao, Y. Han, K. R. Daellenbach, J. G. Slowik, S. M. Platt, F. Canonaco, P. Zotter, R. Wolf, S. M. Pieber, E. A. Bruns, M. Crippa, G. Ciarelli, A. Piazzalunga, M. Schwikowski, G. Abbaszade, J. Schnelle-Kreis, R. Zimmermann, Z. An, S. Szidat, U. Baltensperger, I. El Haddad and A. S. H. Prévôt, High secondary aerosol contribution to particulate pollution during haze events in China, *Nature*, 2014, **514**, 218–222.

21 M. Hallquist, J. C. Wenger, U. Baltensperger, Y. Rudich, D. Simpson, M. Claeys, J. Dommen, N. M. Donahue, C. George, A. H. Goldstein, J. F. Hamilton, H. Herrmann, T. Hoffmann, Y. Iinuma, M. Jang, M. E. Jenkin, J. L. Jimenez, A. Kiendler-Scharr, W. Maenhaut, G. McFiggans, T. F. Mentel, A. Monod, A. S. H. Prévôt, J. H. Seinfeld, J. D. Surratt, R. Szmigielski and J. Wildt, The formation, properties and impact of secondary organic aerosol: current and emerging issues, *Atmos. Chem. Phys.*, 2009, **9**, 5155–5236.

22 S. S. Brown and J. Stutz, Nighttime radical observations and chemistry, *Chem. Soc. Rev.*, 2012, **41**, 6405–6447.

23 R. Atkinson, Atmospheric chemistry of VOCs and NOx, *Atmos. Environ.*, 2000, **34**, 2063–2101.

24 W. P. Carter, Development of Ozone Reactivity Scales for Volatile Organic Compounds, *Air Waste*, 1994, **44**, 881–899.

25 D. R. Gentner, S. H. Jathar, T. D. Gordon, R. Bahreini, D. A. Day, I. El Haddad, P. L. Hayes, S. M. Pieber, S. M. Platt, J. de Gouw, A. H. Goldstein, R. A. Harley, J. L. Jimenez, A. S. H. Prévôt and A. L. Robinson, Review of Urban Secondary Organic Aerosol Formation from Gasoline and Diesel Motor Vehicle Emissions, *Environ. Sci. Technol.*, 2017, **51**, 1074–1093.

26 S. M. Platt, I. E. Haddad, S. M. Pieber, R.-J. Huang, A. A. Zardini, M. Clairotte, R. Suarez-Bertoa, P. Barmet, L. Pfaffenberger, R. Wolf, J. G. Slowik, S. J. Fuller, M. Kalberer, R. Chirico, J. Dommen, C. Astorga, R. Zimmermann, N. Marchand, S. Hellebust, B. Temime-Roussel, U. Baltensperger and A. S. H. Prévôt, Two-stroke scooters are a dominant source of air pollution in many cities, *Nat. Commun.*, 2014, **5**, 3749.

27 J. K. Kodros, D. K. Papanastasiou, M. Paglione, M. Masiol, S. Squizzato, K. Florou, K. Skyllakou, C. Kaltsonoudis, A. Nenes and S. N. Pandis, Rapid dark aging of biomass

burning as an overlooked source of oxidized organic aerosol, *Proc. Natl. Acad. Sci. U.S.A.*, 2020, **117**, 33028–33033.

28 A. Hartikainen, P. Tiitta, M. Ihalainen, P. Yli-Pirilä, J. Orasche, H. Czech, M. Kortelainen, H. Lamberg, H. Suhonen, H. Koponen, L. Hao, R. Zimmermann, J. Jokiniemi, J. Tissari and O. Sippula, Photochemical transformation of residential wood combustion emissions: dependence of organic aerosol composition on OH exposure, *Atmos. Chem. Phys.*, 2020, **20**, 6357–6378.

29 A. H. Hartikainen, M. Ihalainen, P. Yli-Pirilä, L. Hao, M. Kortelainen, S. M. Pieber and O. Sippula, Photochemical transformation and secondary aerosol formation potential of Euro6 gasoline and diesel passenger car exhaust emissions, *J. Aerosol Sci.*, 2023, **171**, 106159.

30 Y.-S. Lau, H.-Y. Poon, B. Organ, H.-C. Chuang, M.-N. Chan, H. Guo, S. S. H. Ho and K.-F. Ho, Toxicological effects of fresh and aged gasoline exhaust particles in Hong Kong, *J. Hazard. Mater.*, 2023, **441**, 129846.

31 M. Krapf, L. Künzi, S. Allenbach, E. A. Bruns, I. Gavarini, I. El-Haddad, J. G. Slowik, A. S. H. Prévôt, L. Drinovec, G. Močnik, L. Dümbgen, M. Salathe, N. Baumlin, C. Sioutas, U. Baltensperger, J. Dommen and M. Geiser, Wood combustion particles induce adverse effects to normal and diseased airway epithelia, *Environ. Sci.: Processes Impacts*, 2017, **19**, 538–548.

32 S. Offer, E. Hartner, S. Di Bucchianico, C. Bisig, S. Bauer, J. Pantzke, E. J. Zimmermann, X. Cao, S. Binder, E. Kuhn, A. Huber, S. Jeong, U. Käfer, P. Martens, A. Mesceriakovas, J. Bendl, R. Brejcha, A. Buchholz, D. Gat, T. Hohaus, N. Rastak, G. Jakobi, M. Kalberer, T. Kanashova, Y. Hu, C. Ogris, A. Marsico, F. Theis, M. Pardo, T. Gröger, S. Oeder, J. Orasche, A. Paul, T. Ziehm, Z.-H. Zhang, T. Adam, O. Sippula, M. Sklorz, J. Schnelle-Kreis, H. Czech, A. Kiendler-Scharr, Y. Rudich and R. Zimmermann, Effect of Atmospheric Aging on Soot Particle Toxicity in Lung Cell Models at the Air-Liquid Interface: Differential Toxicological Impacts of Biogenic and Anthropogenic Secondary Organic Aerosols (SOAs), *Environ. Health Perspect.*, 2022, **130**, 27003.

33 M. I. Gilmour, J. D. Krug, S. H. Gavett, M. Hazari, D. M. DeMarini and D. L. Costa, Complex Air Pollution Mixtures Formed by Irradiation of Hydrocarbons Elicit an Array of Toxicological Responses, *Environ. Sci. Technol.*, 2018, **52**, 2429–2431.

34 S. Pye, S. Bradley, N. Hughes, J. Price, D. Welsby and P. Ekins, An equitable redistribution of unburnable carbon, *Nat. Commun.*, 2020, **11**, 3968.

35 P. Martens, H. Czech, J. Tissari, M. Ihalainen, H. Suhonen, M. Sklorz, J. Jokiniemi, O. Sippula and R. Zimmermann, Emissions of Gases and Volatile Organic Compounds from Residential Heating: A Comparison of Brown Coal Briquettes and Logwood Combustion, *Energy Fuels*, 2021, **35**, 14010–14022.

36 T. Brunner, G. Wuercher and I. Obernberger, 2-Year field operation monitoring of electrostatic precipitators for residential wood heating systems, *Biomass Bioenergy*, 2018, **111**, 278–287.

37 A. Paul, Z. Fang, P. Martens, A. Mukherjee, G. Jakobi, M. Ihalainen, M. Kortelainen, M. Somero, P. Yli-Pirilä, T. Hohaus, H. Czech, M. Kalberer, O. Sippula, Y. Rudich, R. Zimmermann and A. Kiendler-Scharr, Formation of secondary aerosol from emissions of a Euro 6-compliant gasoline vehicle with particle filter, *Environ. Sci.: Atmos.*, under review.

38 M. Ihalainen, P. Tiitta, H. Czech, P. Yli-Pirilä, A. Hartikainen, M. Kortelainen, J. Tissari, B. Stengel, M. Sklorz, H. Suhonen, H. Lamberg, A. Leskinen, A. Kiendler-Scharr, H. Harndorf, R. Zimmermann, J. Jokiniemi and O. Sippula, A novel high-volume Photochemical Emission Aging flow tube Reactor (PEAR), *Aerosol Sci. Technol.*, 2019, **53**, 276–294.

39 P. Barmet, J. Dommen, P. F. DeCarlo, T. Tritscher, A. P. Praplan, S. M. Platt, A. S. H. Prévôt, N. M. Donahue and U. Baltensperger, OH clock determination by proton transfer reaction mass spectrometry at an environmental chamber, *Atmos. Meas. Tech.*, 2012, **5**, 647–656.

40 R. Li, B. B. Palm, A. M. Ortega, J. Hlywiak, W. Hu, Z. Peng, D. A. Day, C. Knote, W. H. Brune, J. A. de Gouw and J. L. Jimenez, Modeling the radical chemistry in an oxidation flow reactor: radical formation and recycling, sensitivities, and the OH exposure estimation equation, *J. Phys. Chem. A*, 2015, **119**, 4418–4432.

41 Z. Peng, J. Lee-Taylor, J. J. Orlando, G. S. Tyndall and J. L. Jimenez, Organic peroxy radical chemistry in oxidation flow reactors and environmental chambers and their atmospheric relevance, *Atmos. Chem. Phys.*, 2019, **19**, 813–834.

42 Z. Peng and J. L. Jimenez, Radical chemistry in oxidation flow reactors for atmospheric chemistry research, *Chem. Soc. Rev.*, 2020, **49**, 2570–2616.

43 B. B. Palm, P. Campuzano-Jost, A. M. Ortega, D. A. Day, L. Kaser, W. Jud, T. Karl, A. Hansel, J. F. Hunter, E. S. Cross, J. H. Kroll, Z. Peng, W. H. Brune and J. L. Jimenez, In situ secondary organic aerosol formation from ambient pine forest air using an oxidation flow reactor, *Atmos. Chem. Phys.*, 2016, **16**, 2943–2970.

44 E. Schneider, H. Czech, O. Popovicheva, M. Chichaeva, V. Kobelev, N. Kasimov, T. Minkina, C. P. Rüger and R. Zimmermann, Mass spectrometric analysis of unprecedented high levels of carbonaceous aerosol particles long-range transported from wildfires in the Siberian Arctic, *Atmos. Chem. Phys.*, 2024, **24**, 553–576.

45 Z. Yang, N. T. Tsona, J. Li, S. Wang, L. Xu, B. You and L. Du, Effects of NOx and SO2 on the secondary organic aerosol formation from the photooxidation of 1,3,5-trimethylbenzene: A new source of organosulfates, *Environ. Pollut.*, 2020, **264**, 114742.

46 M. Passananti, L. Kong, J. Shang, Y. Dupart, S. Perrier, J. Chen, D. J. Donaldson and C. George, Organosulfate Formation through the Heterogeneous Reaction of Sulfur Dioxide with Unsaturated Fatty Acids and Long-Chain Alkenes, *Angew. Chem.*, 2016, **55**, 10336–10339.

47 C. He, Z. Fang, Y. Li, C. Jiang, S. Zhao, C. Xu, Y. Zhang and Q. Shi, Ionization selectivity of electrospray and atmospheric pressure photoionization FT-ICR MS for

petroleum refinery wastewater dissolved organic matter, *Environ. Sci.: Processes Impacts*, 2021, **23**, 1466–1475.

48 A. E. Perring, S. E. Pusede and R. C. Cohen, An observational perspective on the atmospheric impacts of alkyl and multifunctional nitrates on ozone and secondary organic aerosol, *Chem. Rev.*, 2013, **113**, 5848–5870.

49 D. A. Day, M. B. Dillon, P. J. Wooldridge, J. A. Thornton, R. S. Rosen, E. C. Wood and R. C. Cohen, On alkyl nitrates, O 3 and the "missing NO y ", *J. Geophys. Res.*, 2003, **108**, 4501.

50 H. S. Kenagy, T. L. Sparks, P. J. Wooldridge, A. J. Weinheimer, T. B. Ryerson, D. R. Blake, R. S. Hornbrook, E. C. Apel and R. C. Cohen, Evidence of Nighttime Production of Organic Nitrates During SEAC 4 RS, FRAPPÉ, and KORUS-AQ, *Geophys. Res. Lett.*, 2020, **47**, e2020GL087860.

51 J. Yang, W. C. Au, H. Law, C. H. Lam and T. Nah, Formation and evolution of brown carbon during aqueous-phase nitrate-mediated photooxidation of guaiacol and 5-nitroguaiacol, *Atmos. Environ.*, 2021, **254**, 118401.

52 M. Pardo, S. Offer, E. Hartner, S. Di Bucchianico, C. Bisig, S. Bauer, J. Pantzke, E. J. Zimmermann, X. Cao, S. Binder, E. Kuhn, A. Huber, S. Jeong, U. Käfer, E. Schneider, A. Msceriakovas, J. Bendl, R. Brejcha, A. Buchholz, D. Gat, T. Hohaus, N. Rastak, E. Karg, G. Jakobi, M. Kalberer, T. Kanashova, Y. Hu, C. Ogris, A. Marsico, F. Theis, T. Shalit, T. Gröger, C. P. Rüger, S. Oeder, J. Orasche, A. Paul, T. Ziehm, Z.-H. Zhang, T. Adam, O. Sippula, M. Sklorz, J. Schnelle-Kreis, H. Czech, A. Kiendler-Scharr, R. Zimmermann and Y. Rudich, Exposure to naphthalene and β-pinene-derived secondary organic aerosol induced divergent changes in transcript levels of BEAS-2B cells, *Environ. Int.*, 2022, **166**, 107366.

53 M. Li, J. Li, Y. Zhu, J. Chen, M. O. Andreae, U. Pöschl, H. Su, M. Kulmala, C. Chen, Y. Cheng and J. Zhao, Highly oxygenated organic molecules with high unsaturation formed upon photochemical aging of soot, *Chem*, 2022, **8**, 2688–2699.

54 M. Xie, X. Chen, M. D. Hays, M. Lewandowski, J. Offenberg, T. E. Kleindienst and A. L. Holder, Light Absorption of Secondary Organic Aerosol: Composition and Contribution of Nitroaromatic Compounds, *Environ. Sci. Technol.*, 2017, **51**, 11607–11616.

55 Y. Zeng, Y. Ning, Z. Shen, L. Zhang, T. Zhang, Y. Lei, Q. Zhang, G. Li, H. Xu, S. S. H. Ho and J. Cao, The Roles of N, S, and O in Molecular Absorption Features of Brown Carbon in PM 2.5 in a Typical Semi-Arid Megacity in Northwestern China, *J. Geophys. Res.: Atmos.*, 2021, **126**, e2021JD034791.

56 R. Wu, S. Pan, Y. Li and L. Wang, Atmospheric oxidation mechanism of toluene, *J. Phys. Chem. A*, 2014, **118**, 4533–4547.

57 V. J. Baboomian, Y. Gu and S. A. Nizkorodov, Photodegradation of Secondary Organic Aerosols by Long-Term Exposure to Solar Actinic Radiation, *ACS Earth Space Chem.*, 2020, **4**, 1078–1089.

58 M. Brüggemann, R. Xu, A. Tilgner, K. C. Kwong, A. Mutzel, H. Y. Poon, T. Otto, T. Schaefer, L. Poulain, M. N. Chan

and H. Herrmann, Organosulfates in Ambient Aerosol: State of Knowledge and Future Research Directions on Formation, Abundance, Fate, and Importance, *Environ. Sci. Technol.*, 2020, **54**, 3767–3782.

59 A. M. K. Hansen, J. Hong, T. Raatikainen, K. Kristensen, A. Ylisirniö, A. Virtanen, T. Petäjä, M. Glasius and N. L. Prisle, Hygroscopic properties and cloud condensation nuclei activation of limonene-derived organosulfates and their mixtures with ammonium sulfate, *Atmos. Chem. Phys.*, 2015, **15**, 14071–14089.

60 P. Lin, J. Liu, J. E. Shilling, S. M. Kathmann, J. Laskin and A. Laskin, Molecular characterization of brown carbon (BrC) chromophores in secondary organic aerosol generated from photo-oxidation of toluene, *Phys. Chem. Chem. Phys.*, 2015, **17**, 23312–23325.

61 E. Schneider, H. Czech, O. Popovicheva, H. Lütdke, J. Schnelle-Kreis, T. Khodzher, C. P. Rüger and R. Zimmermann, Molecular Characterization of Water-Soluble Aerosol Particle Extracts by Ultrahigh-Resolution Mass Spectrometry: Observation of Industrial Emissions and an Atmospherically Aged Wildfire Plume at Lake Baikal, *ACS Earth Space Chem.*, 2022, **6**, 1095–1107.

62 D. G. Poppendieck, D. Rim and A. K. Persily, Ultrafine particle removal and ozone generation by in-duct electrostatic precipitators, *Environ. Sci. Technol.*, 2014, **48**, 2067–2074.

63 A. Furey, M. Moriarty, V. Bane, B. Kinsella and M. Lehane, Ion suppression; a critical review on causes, evaluation, prevention and applications, *Talanta*, 2013, **115**, 104–122.

64 P. K. Hopke and X. Querol, Is Improved Vehicular NOx Control Leading to Increased Urban NH3 Emissions?, *Environ. Sci. Technol.*, 2022, **56**, 11926–11927.

65 S. M. Pieber, N. K. Kumar, F. Klein, P. Comte, D. Bhattu, J. Dommen, E. A. Bruns, D. Kılıç, I. El Haddad, A. Keller, J. Czerwinski, N. Heeb, U. Baltensperger, J. G. Slowik and A. S. H. Prévôt, Gas-phase composition and secondary organic aerosol formation from standard and particle filter-retrofitted gasoline direct injection vehicles investigated in a batch and flow reactor, *Atmos. Chem. Phys.*, 2018, **18**, 9929–9954.

66 Z. Li, S. A. Nizkorodov, H. Chen, X. Lu, X. Yang and J. Chen, Nitrogen-containing secondary organic aerosol formation by acrolein reaction with ammonia/ammonium, *Atmos. Chem. Phys.*, 2019, **19**, 1343–1356.

67 Y.-H. Lin, M. Arashiro, E. Martin, Y. Chen, Z. Zhang, K. G. Sexton, A. Gold, I. Jaspers, R. C. Fry and J. D. Surratt, Isoprene-Derived Secondary Organic Aerosol Induces the Expression of Oxidative Stress Response Genes in Human Lung Cells, *Environ. Sci. Technol. Lett.*, 2016, **3**, 250–254.

68 L. Yu, J. Smith, A. Laskin, K. M. George, C. Anastasio, J. Laskin, A. M. Dillner and Q. Zhang, Molecular transformations of phenolic SOA during photochemical aging in the aqueous phase: competition among oligomerization, functionalization, and fragmentation, *Atmos. Chem. Phys.*, 2016, **16**, 4511–4527.

69 C. L. Heald, J. H. Kroll, J. L. Jimenez, K. S. Docherty, P. F. DeCarlo, A. C. Aiken, Q. Chen, S. T. Martin,

D. K. Farmer and P. Artaxo, A simplified description of the evolution of organic aerosol composition in the atmosphere, *Geophys. Res. Lett.*, 2010, **37**, L08803.

70 P. Lin, P. K. Aiona, Y. Li, M. Shiraiwa, J. Laskin, S. A. Nizkorodov and A. Laskin, Molecular Characterization of Brown Carbon in Biomass Burning Aerosol Particles, *Environ. Sci. Technol.*, 2016, **50**, 11815–11824.

71 M. Brüggemann, L. Poulain, A. Held, T. Stelzer, C. Zuth, S. Richters, A. Mutzel, D. van Pinxteren, Y. Iinuma, S. Katkevica, R. Rabe, H. Herrmann and T. Hoffmann, Real-time detection of highly oxidized organosulfates and BSOA marker compounds during the F-BEACh 2014 field study, *Atmos. Chem. Phys.*, 2017, **17**, 1453–1469.

72 M. S. Shalamzari, A. Kahnt, R. Vermeylen, T. E. Kleindienst, M. Lewandowski, F. Cuyckens, W. Maenhaut and M. Claeys, Characterization of polar organosulfates in secondary organic aerosol from the green leaf volatile 3-Z-hexenal, *Environ. Sci. Technol.*, 2014, **48**, 12671–12678.

73 Y. Han, X. Zhang, L. Li, Y. Lin, C. Zhu, N. Zhang, Q. Wang and J. Cao, Enhanced Production of Organosulfur Species during a Severe Winter Haze Episode in the Guanzhong Basin of Northwest China, *Environ. Sci. Technol.*, 2023, **57**, 8708–8718.

74 X. K. Wang, S. Rossignol, Y. Ma, L. Yao, M. Y. Wang, J. M. Chen, C. George and L. Wang, Molecular characterization of atmospheric particulate organosulfates in three megacities at the middle and lower reaches of the Yangtze River, *Atmos. Chem. Phys.*, 2016, **16**, 2285–2298.

75 A. Schmalenberger, W. Pritzkow, J. J. Ojeda and M. Noll, Characterization of main sulfur source of wood-degrading basidiomycetes by S K-edge X-ray absorption near edge spectroscopy (XANES), *Int. Biodeterior. Biodegrad.*, 2011, **65**, 1215–1223.

76 B. R. Simoneit, Biomass burning—a review of organic tracers for smoke from incomplete combustion, *Appl. Geochem.*, 2002, **17**, 129–162.

77 T. E. Kleindienst, T. S. Conver, C. D. McIver and E. O. Edney, Determination of Secondary Organic Aerosol Products from the Photooxidation of Toluene and their Implications in Ambient PM 2.5, *J. Atmos. Chem.*, 2004, **47**, 79–100.

78 H. Wu, J. W. Taylor, J. M. Langridge, C. Yu, J. D. Allan, K. Szpek, M. I. Cotterell, P. I. Williams, M. Flynn, P. Barker, C. Fox, G. Allen, J. Lee and H. Coe, Rapid transformation of ambient absorbing aerosols from West African biomass burning, *Atmos. Chem. Phys.*, 2021, **21**, 9417–9440.

79 X. Feng, J. Wang, S. Teng, X. Xu, B. Zhu, J. Wang, X. Zhu, M. A. Yurkin and C. Liu, Can light absorption of black carbon still be enhanced by mixing with absorbing materials?, *Atmos. Environ.*, 2021, **253**, 118358.